

1 **The formation and geometry characteristics of boulder bars due to**
2 **outburst flood triggered by the overtopped landslide dam failure**

3 Xiangang Jiang^{✉1} · Haiguang Cheng¹ · Lei Gao² · Weiming Liu³

4 ¹College of Civil Engineering, Sichuan Agricultural University, Dujiangyan, Chengdu 611830,
5 China

6 ²Key Laboratory of Ministry of Education for Geomechanics and Embankment Engineering,
7 Hohai University, Nanjing 210098, China

8 ³Key Laboratory of Mountain Hazards and Earth Surface Process, Institute of Mountain Hazards
9 and Environment, Chinese Academy of Sciences, Chengdu 610041, China

10 Correspondence to: Xiangang Jiang (✉E-mail: jxgjim@163.com)

11 **Abstract**

12 Boulder bars are a common form of riverbed morphology that could be affected by
13 landslide dams. However, few studies have focused on the formation and geometry
14 characteristics of boulder bars due to outburst floods triggered by landslide dam failure.
15 In such way, eight group landslide dam failure experiments with movable bed length
16 for 4 to 7 times of dam length with 25 boulder bars were carried out. In addition, 38
17 boulder bars formed in the field triggered by four landslide dam failures were
18 investigated. The aim of this paper is to study the formation and geometry
19 characteristics of boulder bars along the riverbeds. The results show that boulder bars
20 are formed after peak discharge of outburst flow. The number of boulder bars is 0.4 to
21 1.0 times the ratio of river bed length to dam bottom length. Besides, boulder bars have
22 the characteristic of lengthening towards upstream during the failure process. Boulder

23 bar's upstream edge has a more extensive development than boulder bar downstream
24 edge. The length of a boulder bar along the channel changes faster than the boulder
25 bar's width and height. After the dam failure, the boulder bar's length is about 8 to 14
26 times of width. The relationship between ratio of boulder bar length to width and
27 boulder bar's dimensionless length could be described with a hyperbolic equation. The
28 dimensionless area of boulder bar increases linearly with the dimensionless area of the
29 river section, and the linear ratio is about 0.5. With the field data, it demonstrates the
30 formation and geometry characteristics of boulder bars in tests are consistent with the
31 field boulder bars. Therefore, the results in this paper are credible, and can be applied
32 to the river bed's geomorphological characteristics analysis triggered by overtopped
33 landslide dam failure. The plenty of experimental and field data could contribute to the
34 community for the boulder bars' research.

35 **Keywords**

36 Landslide dam · Overtopping failure · Boulder bar · Formation and geometry
37 characteristics

38 **1. Introduction**

39 Activities such as rainfalls and earthquakes often cause landslides, which block
40 the river to form a water-retaining body similar to a reservoir dam, called a landslide
41 dam (Takahashi, 2007; Costa and Schuster, 1988; Casagli, 2003). According to
42 statistics, 85 % of the dams failed within one year after formations, and more than 50 %
43 of the dams breached with overtopping mode (Costa and Schuster, 1988). When the

44 dam breach, the storage water erupt and flown carrying the dam materials to the
45 downstream riverbed, which may change original riverbed geomorphology.

46 Many studies on the influence of flood geomorphology and sedimentary
47 characteristics have proved that the outburst flood energy is huge, and it can entrain and
48 transport materials of various sizes, from clay to boulders. A large number of boulders
49 gather in the river to form bars, namely boulder bars. The downstream riverbed's
50 geomorphology will be significantly affected and undergo significant changes (Lamb
51 and Fonstad, 2010; Maizels, 1997; Russell and Knudsen, 1999; Marren and Schuh,
52 2009; Benito and O'Connor, 2003; Carling, 2013; Wu et al., 2020). Boulder bars are
53 one common landform formed during the outburst flood evolution (Turzewski et al.,
54 2019; Jiang and Wei, 2020; Wu et al., 2020). For example, in the 2000 year, Yigong
55 outburst flood, due to its huge lake storage, formed many huge boulder bars on the river
56 bed. The boulder bars had a significant impact on the development of the river bedform.
57 And Wu et al. (2020) investigated the impact of this event on river morphology and
58 analyzed the shapes and geometric characteristics of the boulder bars caused by the
59 overtopping flood. And they found that the boulder bar components are poorly sorted.
60 Turzewski et al. (2019) studied the particle gradation of the boulder bars during the
61 Yigong River landslide dam failure process. They found that the boulder bars' particle
62 sizes decrease along the lower reaches of the river bed. But they did not analyze the
63 evolution characteristics of boulder bar's size in detail. Lamb and Fonstad (2010)
64 suggested that the rising and falling stages of the outburst flood had a greater impact on
65 riverbed geomorphology and analyzed the characteristics of the median diameter of

66 material in boulder bar.

67 The boulder bars triggered by landslide dam failure are formed under a
68 nonequilibrium sediment transport condition. Sediment pulses delivered to downstream
69 are dispersive under this condition. It is very different from river dunes under steady
70 flow conditions, which is an equilibrium sediments transport condition, and the
71 sandbars maintain their geometry when they migrate downstream. It means that the
72 boulder bars' shape and geometry size are variation during its formation process.
73 Furthermore, the formation of boulder bars is different from sandbars which formed by
74 translative depositional processes (Mohrig and Smith, 1996; Ashworth et al., 2000;
75 Shaw and McElroy, 2016).

76 Because lack of investigations about the growth characteristics of boulder bars
77 during the landslide dam failure process in the field, some researchers had conducted
78 landslide dam failure experiments in the lab (Ashworth, 1996; Jiang and Wei, 2020).
79 Ashworth (1996) used flume experiments to study the boulder bar's growth. However,
80 in their experiments, the inflow conditions are quite different from the outburst flood.
81 Therefore, the research results' applicability to the boulder bar formed by the outburst
82 flood remains uncertain. Jiang and Wei (2020) qualitatively analyzed the formation
83 process of boulder bar in the evolution of overtopping outburst floods using dam failure
84 experiments and initially discussed the characteristics of geometric size of boulder bars
85 after dam failure. However, the characteristics of the boulder bar's distribution and
86 geometric size characteristics during the dam failure process have not been analyzed.

87 Above all, there is a common academic consensus that outburst flow triggered by

88 landslide dam failure could change the geomorphology of downstream riverbed.
89 Although, the failure process of the dam and the hydraulic characteristics of the outburst
90 flood, such the characteristics of breaching hydraulic graph, erosion rate and peak
91 discharge (Morris et al., 2009; Jiang and Wei 2018; Jiang, 2019), are clear, the impact
92 of the outburst flood triggered by landslide dam failure on the geomorphology of the
93 downstream riverbed during the failure process and after failure is still lack of research.
94 Boulder bar is the substance occurred during the dam failure process which is an
95 indicator for the variation of riverbed geomorphology. What are the formation
96 characteristics of boulder bars during the dam failure process? And what geometry
97 characteristics of boulder bar are during the dam failure process and after the dam
98 failure? These questions are still not clear and should be answered. Understanding these
99 questions is helpful for predication of riverbed landform influenced by landslide dam
100 failure, and benefit to assessment of stream restoration and river navigation.

101 This paper focuses on the formation processes and the geometrical size
102 characteristics of boulder bars in the downstream channel during and after the
103 overtopping failure process. Firstly, through flume experiments, boulder bars' formation
104 processes on the downstream channel under the dammed lake failure condition were
105 reproduced. Then, based on the experimental data, the development characteristics of
106 boulder bars' upstream and downstream edges were analyzed. Furthermore, statistical
107 analysis of boulder bars geometrical sizes at each moment during and after the failure
108 process, such as length, width, height, volume and area of boulder bar, had been carried
109 out to obtain boulder bars' size characteristics. Finally, compare the distribution and

110 geometry characteristics of the boulder bar formed in the experiment and field to verify
 111 experiment results' reliability. The results can be applied to the river bed's
 112 geomorphological characteristics research affected by the outburst flood triggered by
 113 landslide dam failure. And also, this paper provides a large number of experimental and
 114 field boulder bars' data reference to the analysis of the erosion and accumulation
 115 characteristics of the downstream river channel.

116 **2. Experimental design**

117 **2.1 Model design and experimental materials**

118 The longitudinal profiles of experimental landslide dams were trapezoidal and
 119 triangular. The trapezoidal dam height and crest width were both 0.3 m, and the
 120 triangular dam height was also 0.3 m. In the experiment, river bed slope angle θ was
 121 fixed at 10° , and the landslide dam upstream slope angle α was set to 40° , and the
 122 landslide dam downstream slope angles β were set to five different values. The
 123 moveable bed was set downstream of the model dam, which had a length of 8 m. The
 124 downstream channel bed's length was about 4 to 7 times of dam length along the
 125 channel. The test parameters are shown in Table 1.

126 **Table 1** test parameters

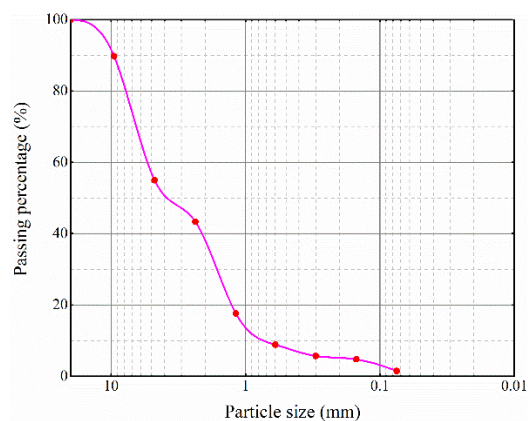
No.	Dam shape	β ($^\circ$)
T1	Trapezoid	10
T2	Trapezoid	15
T3	Trapezoid	20
T4	Trapezoid	25
T5	Trapezoid	30
T6	Tringle	10
T7	Tringle	15
T8	Tringle	20

127 Peng and Zhang (2012) proposed that landslide dam height (H_d), dam bottom
128 width parallel to the channel (W_d), dam volume (V_d), and reservoir volume (V_l) are the
129 key geometric parameters of landslide dam, and proposed a set of dimensionless
130 numbers, $\frac{H_d}{W_d}$, $\frac{V_d^{1/3}}{H_d}$ and $\frac{V_l^{1/3}}{H_d}$, to verify whether the established dam model is
131 consistent with the landslide dam in the field (Zhou et al., 2019). As the field data show
132 that the $\frac{H_d}{W_d}$, $\frac{V_d^{1/3}}{H_d}$ and $\frac{V_l^{1/3}}{H_d}$ are ranged about 0.001 to 2, 0 to 40, and 0 to 20 for filed
133 landslide dam (Zhou et al., 2019). Table 2 shows the dimensionless numbers of the
134 experimental dams, which are all within the acceptable range of the field landslide dams,
135 indicating that the dams in the experiments are relatively close to field landslide dams.
136 **Table 2** landslide dam parameters. The value of $\frac{H_d}{W_d}$ ranges from 0.1 to 0.3, and $\frac{V_d^{1/3}}{H_d}$ and $\frac{V_l^{1/3}}{H_d}$
137 both range from 1 to 2, which all fall within the acceptable range of values of the field landslide
138 dams (Zhou et al., 2019).

No.	H_d (m)	W_d (m)	$\frac{H_d}{W_d}$	$\frac{V_d^{1/3}}{H_d}$	$\frac{V_l^{1/3}}{H_d}$
T1	0.3	2.359	0.127	1.643	1.477
T2	0.3	1.777	0.169	1.513	1.477
T3	0.3	1.482	0.202	1.437	1.477
T4	0.3	1.301	0.231	1.387	1.477
T5	0.3	1.177	0.255	1.350	1.477
T6	0.3	2.059	0.146	1.508	1.477
T7	0.3	1.477	0.203	1.350	1.477
T8	0.3	1.182	0.254	1.254	1.477

139 In the field, the landslide dam and the boulder bars are almost consisted of
140 mixtures. The dam materials used in this study were mixtures of sand and gravels.
141 Considering the grain size effect and the flume space limitation, the maximum sediment
142 particle size was set to 20 mm. The materials used in the tests had a median particle
143 size of $D_{50}=3.8$ mm. A dimensionless parameter measure of the spread in the grain-size

144 distribution, $\sigma_g = d_{90}/d_{10} = 14.3$ represents a wide grain size range of granular materials
145 for landslide dams. While the materials of riverbed are different from that of landslide
146 dam, it is hard to find a general description of the difference. Thus, we designed the
147 materials of riverbed and landslide dam the same for present experiments. Moreover,
148 the compositions of field dam and riverbed can be heterogeneous, i.e. the distribution
149 of coarse particle within landslide dam is inhomogeneity, there is still no quantitative
150 representation of the heterogeneity. Therefore, the coarse particles and fines were mixed
151 uniform, which means the distribution of coarse particles were homogeneous. The
152 channel morphology in nature is complex and diverse, which was not considered in the
153 experiments. Instead, a straight, aequare and flat channel was set, which is helpful to
154 reveal the fundamental mechanism of the formation process and geometric
155 characteristics of boulder bars. The thickness of the riverbed was set to 0.06 m. The
156 gradation curve of material particles' sizes is shown in Fig. 1.

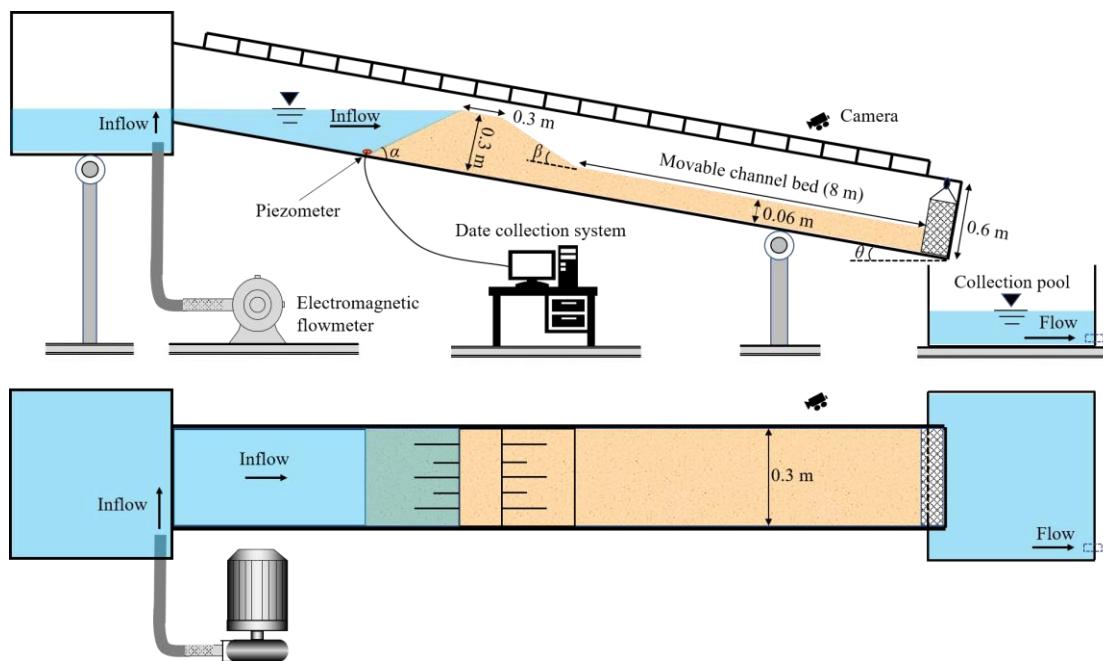


157
158 **Figure 1.** Gradation curve of the dam materials

159 **2.2 Experimental apparatus**

160 The experimental setups are shown in Fig. 2. The flume was 15 m long, 0.3 m
161 wide, and 0.6 m high. The flume slope was adjustable from 10 to 30°. One side of the

162 flume was transparent glass, and scale lines were drawn on the glass to facilitate
 163 observation and recording of experimental phenomena. The inflow discharge upstream
 164 the dam was set as 1.0 L s^{-1} . Under the control of the electromagnetic flowmeter, the
 165 error range could be controlled within $\pm 0.01 \text{ L s}^{-1}$. During the tests, the toe of the dam
 166 upstream slope was set at 4.5 m away from the water supply tank. A baffle with a height
 167 of 6 cm was set at the flume end as a boundary condition. Seven cameras were placed
 168 on the transparent glass side of the flume, one camera was placed on the top of the dam,
 169 and one camera was placed directly behind the flume. A total of nine cameras recorded
 170 the whole experimental phenomena.



171
 172 **Figure. 2.** Experimental setups. (a) Front view of the flume. (b) Top view of the flume.

173 2.3 Measurements

174 In the experiment, using the scale lines on the transparent glass on the side of the
 175 flume, we can accurately read the boulder bars' positions at each moment. Boulder bars'
 176 lengths, widths, and heights could be obtained from the screen. According to the actual

177 boulder bars' geometric characteristics, the boulder bars were divided into several parts,
178 and then the volume calculation formula of the similar geometric body was used to
179 calculate the volume of each part respectively, and finally, the boulder bars' volumes
180 were obtained by summing. The method of obtaining the boulder bar area was the same
181 as that of the volume. After the dam was completely failed, we collected all the boulder
182 bar materials. Then dried and screened silt to obtain the boulder bar material gradation
183 information.

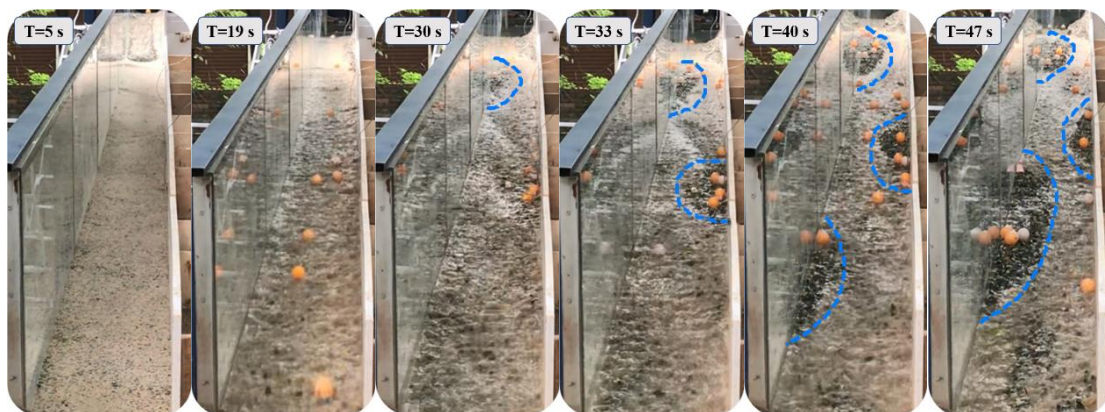
184 **3. Experimental results**

185 **3.1 Formation processes of boulder bars**

186 The formation processes of boulder bars are almost similar for all the tests.
187 Therefore, it takes the T7 test as an example to analyze below in this section, as shown
188 in Fig. 3. When the flow overtopped the dam crest, the outburst flood carried the dam
189 materials to the dam downstream slope ($T=5$ s) and then to the channel bed ($T=19$ s)
190 with outburst flow discharge increasing. It should be noted that although a large number
191 of sediments were transported on the channel bed before the peak discharge, no boulder
192 bar formed on the downstream channel bed. After the moment of peak discharge, the
193 flow discharge gradually weakened, and dam materials were transported to the position
194 near the dam toe. The flow could not transport all the sediments away, and some
195 sediments gradually silted down, then the first boulder bar occurred near the dam toe
196 ($T=30$ s, the boulder bar in the figure is marked with a blue dotted line). After the first
197 boulder bar was formed, the flow direction was changed when water flow bypassed the

198 boulder bar. And the moving sediments still moved along the original direction due to
199 inertia, which causes sediments piled up to form the second boulder bar on the opposite
200 side of the first boulder bar (T=33s).

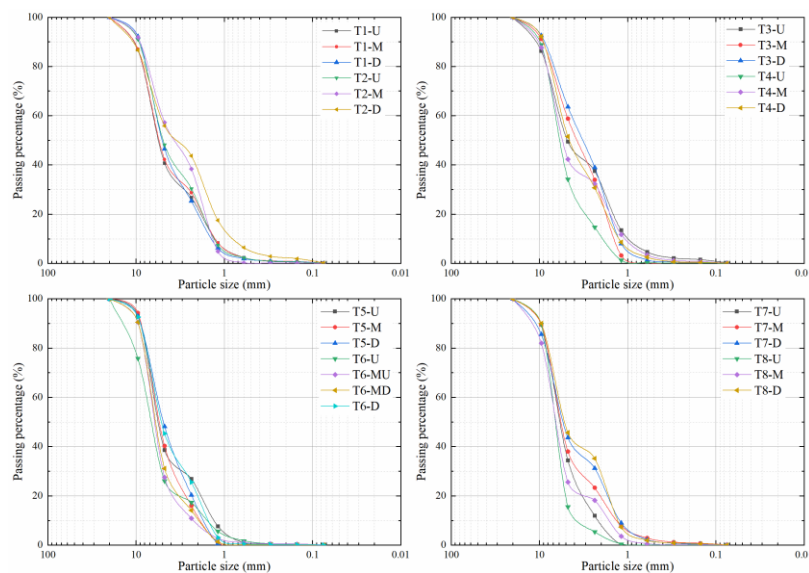
201 Similarly, the first and second boulder bars affected the formation of the boulder
202 bar downstream. Eventually, boulder bars were scattered on both sides of the channel,
203 forming a meandering channel downstream (T=40 and 47 s). This phenomenon is in
204 good agreement with the field boulder bars along the Yigong river (Wu et al., 2020). In
205 addition, the Froude number of flows on the downstream were all larger than 2.5 during
206 the bars' formation process, indicating these bars were formed in a supercritical flow
207 (diffusive) condition. It suggests that boulder bars were formed on dispersive sediment
208 pulses which delivered from the upstream during the landslide dam failure process.
209 (Shaw and McElroy, 2016).



210
211 **Figure. 3.** The riverbed morphology at six different moments during the boulder bars' formations
212 and growths process for the T7 experiment. The boulder bars in the figure are marked with blue
213 dotted lines.

214 Turzewski et al. (2019) measured the sizes of field boulder bars. They found that
215 grain sizes of boulder bars decrease downstream. In this experiment, sediments in

216 boulder bars after dam failure from different locations were collected. After sieving the
 217 sediments, the gradation curves of the materials were obtained as shown in Fig. 4. The
 218 figures show that the contents of fines in the compositions become much less and their
 219 mean diameters become larger than the initial sediments. It means that in the boulder
 220 bars coarse sediment tends to comprise much of the bar material. Meanwhile, the figure
 221 indicates that as the distance between the boulder bar and the dam increases, the particle
 222 diameter in the bars shows a decreasing trend. This feature is consistent with the
 223 description of Turzewski et al. (2019).



224
 225 **Figure 4.** Gradation curve of the boulder bar materials. Notation: U, M, D, MU, and MD, represent
 226 the boulder bar near the upstream reaches, the boulder bar near the middle reaches, the boulder bar
 227 near the downstream reaches, the boulder bar near the middle-upstream reaches, and the boulder
 228 bar near the middle-downstream reaches, respectively.

229

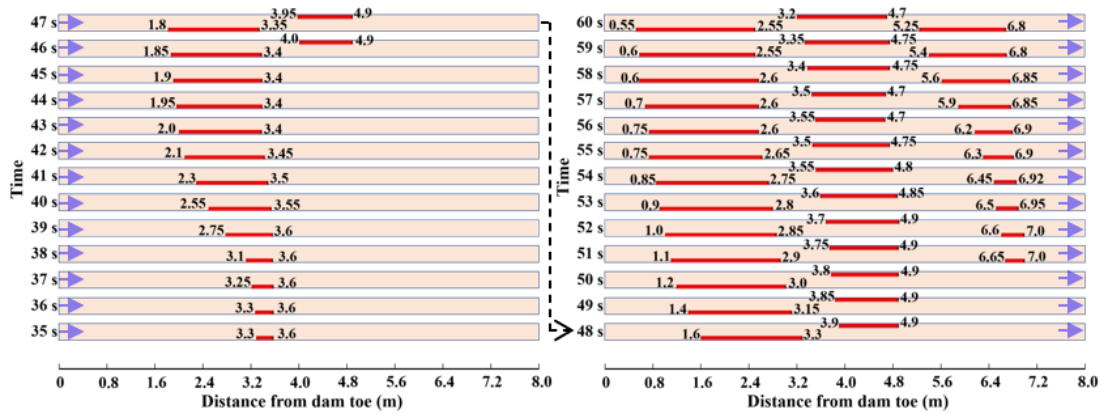
230 3.2 Evolution characteristics of the boulder bars during dam failure process

231 Figure. 5 shows boulder bars' locations on the channel bed during the dam failure
 232 process. The red lines in the figure represent the boulder bars' outlines, and the orange

233 rectangles represent the channels. It clearly shows the formation sequences of boulder
234 bars at different locations. That is, boulder bars were formed first near the dams
235 (upstream reaches of riverbed), and the farther from the dam toe, the later the boulder
236 bar was formed, which is consistent with the content of Sect. 3.1. Boulder bars near the
237 downstream dam toes are all located on the dam breach side across the river. This
238 characteristic has also been found in Chen et al. (2015).

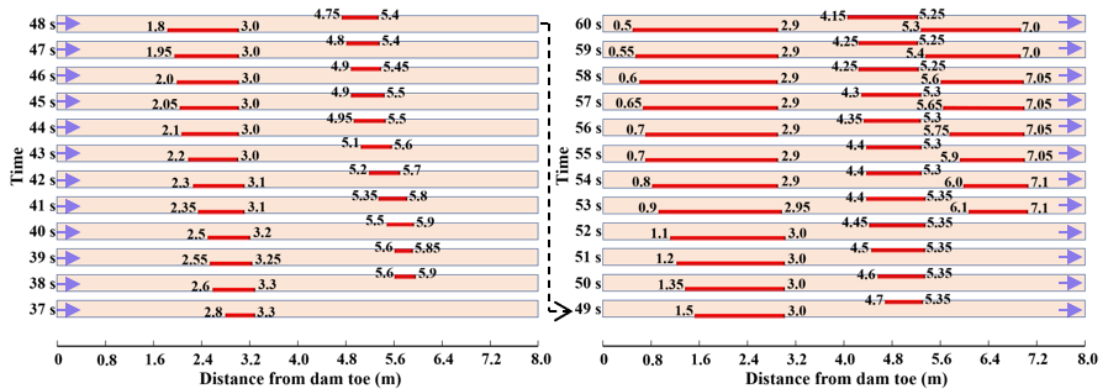
239 According to the boulder bars' formation sequences, the channel bed's boulder bars
240 were divided into three types: I. the boulder bar near the upstream reaches, that is, the
241 boulder bar near the dam toe; II. the boulder bar at the middle reaches; and III. the
242 boulder bar near the downstream reaches. Figure 5 shows that the upstream edges of
243 the boulder bars of type I for all the tests basically moved toward the dams with time
244 development. The movement directions of the downstream edges of boulder bars of
245 type I showed a little different: for T1, T2 and T5, the boulder bars' downstream edges
246 moved toward the dam toes, from a distance from the downstream toe of 3.6 to 2.55 m,
247 3.3 to 2.9 m and 3.7 to 3.4 m, respectively, as shown in Fig.5 (a), (b) and (e); for T6,
248 T7, and T8, the boulder bars' downstream edges first moved away from the dam toes
249 and then moved toward the dam toes, and the downstream edges move forward
250 compared to the original location. However, the distance they moved is 0.1 to 0.2 m, as
251 shown in Fig.5 (f), (g), and (h); for T3 and T4, the boulder bars' downstream edges
252 positions remained almost unchanged, see Fig.5(c) and (d). No matter how the
253 downstream edge positions of the boulder bars type I changed, there is a common
254 feature: compared with the initial positions of the boulder bars, the downstream edges

255 almost remained original locations, and the movement distances were much smaller
 256 than those of boulder bars' upstream edges. The lengths of the boulder bars of type I
 257 increased with the failure time. It can be seen that the sediments on the boulder bars'
 258 upstream edges played a great role in the length developments of type I boulder bars.



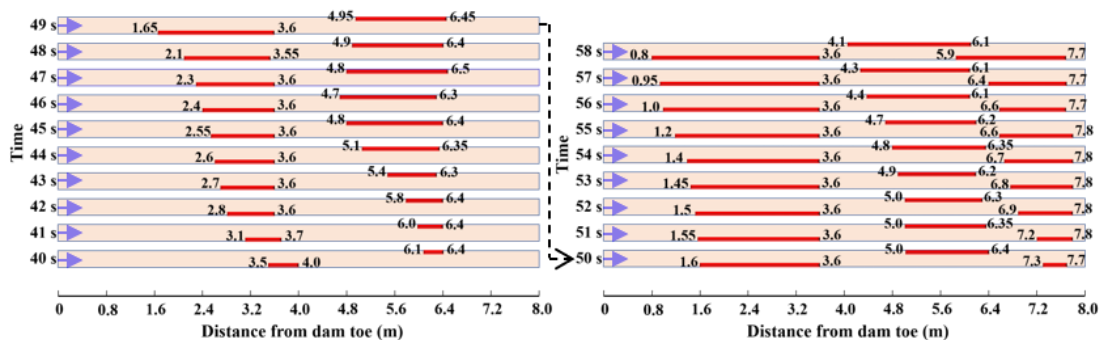
259
 260

(a)



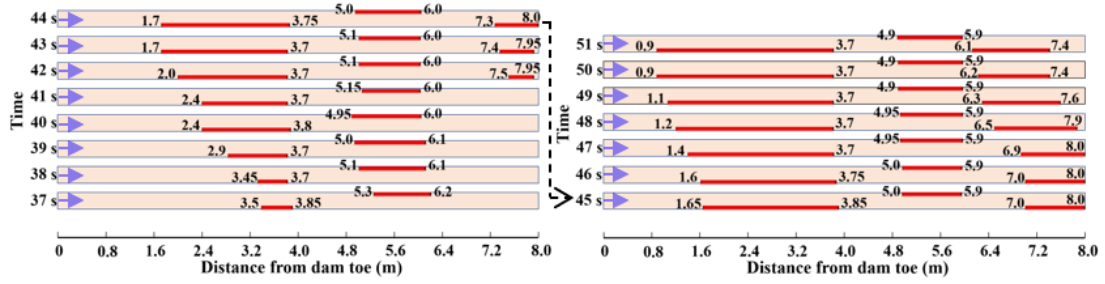
261
 262

(b)



263
 264

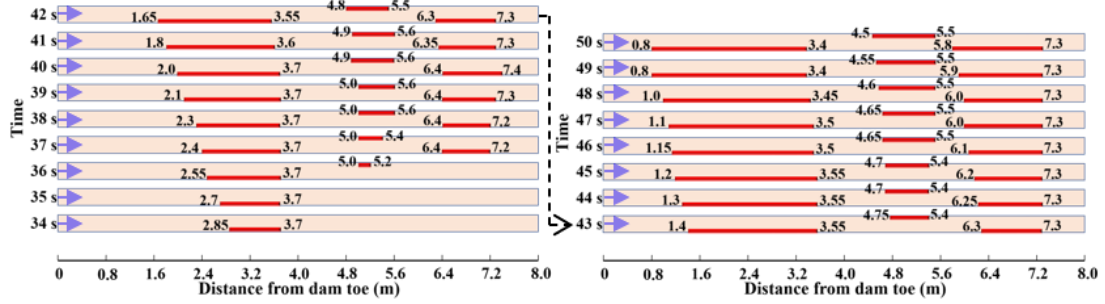
(c)



265

266

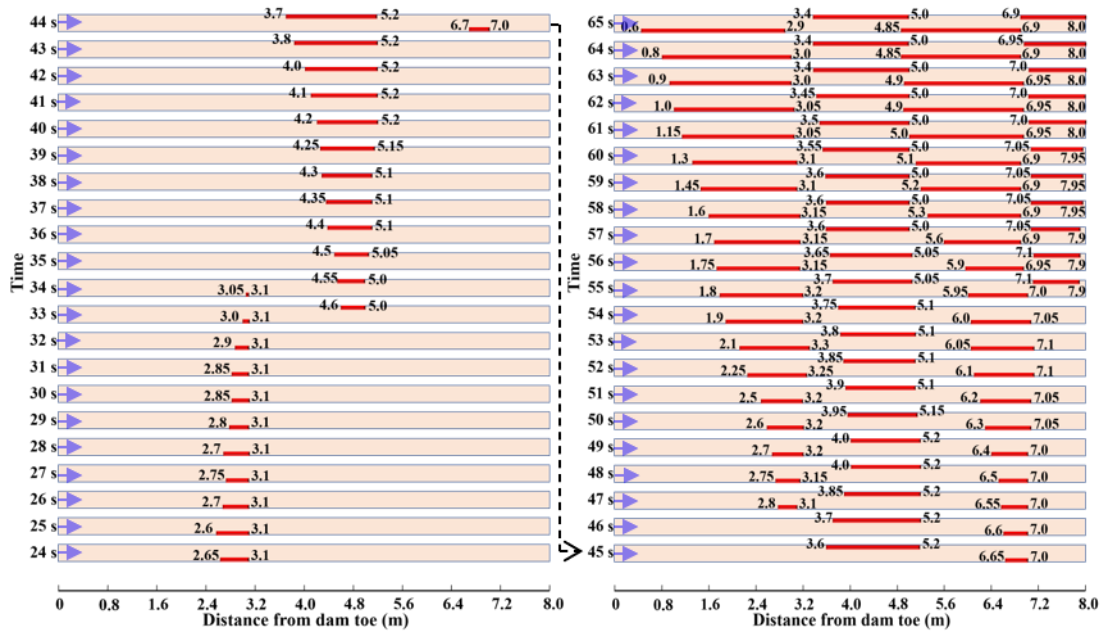
(d)



267

268

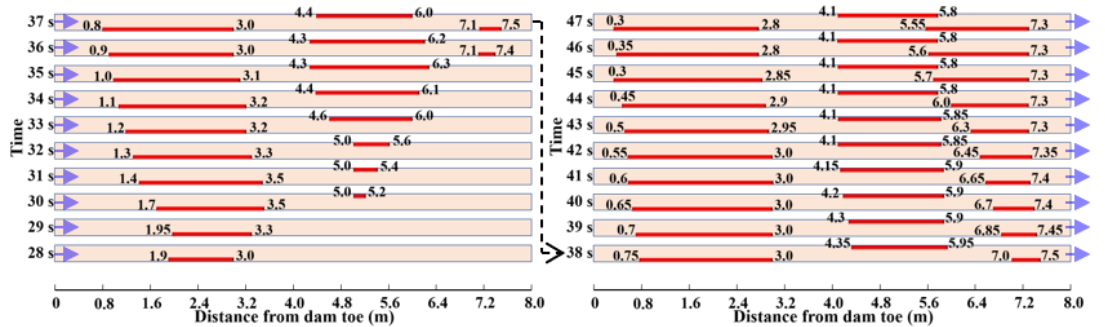
(e)



269

270

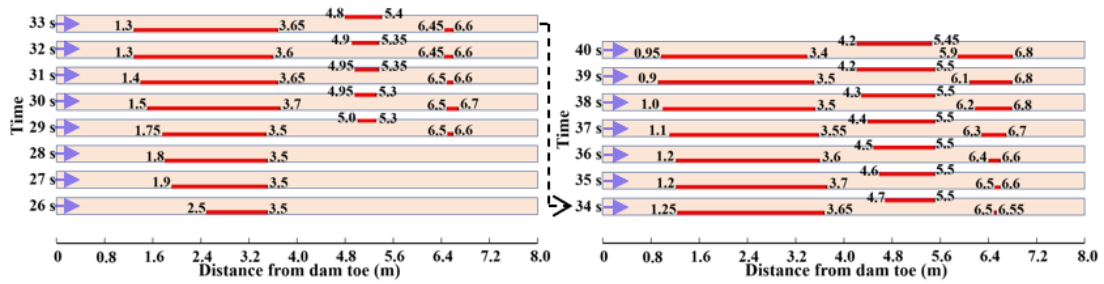
(f)



271

272

(g)



273

274

(h)

275 **Figure. 5.** The boulder bars' locations during the dam failure process. Notation: (a) to (h) represent
 276 the boulder bars' locations for T1-T8 tests, respectively. The red lines in the figure represent the
 277 boulder bars, and the orange rectangles represent the channels. And, the purple arrow represents the
 278 direction of flow. The numbers at both ends of the red lines represent the distances between the
 279 upstream and downstream edges of boulder bars and the dam toe.

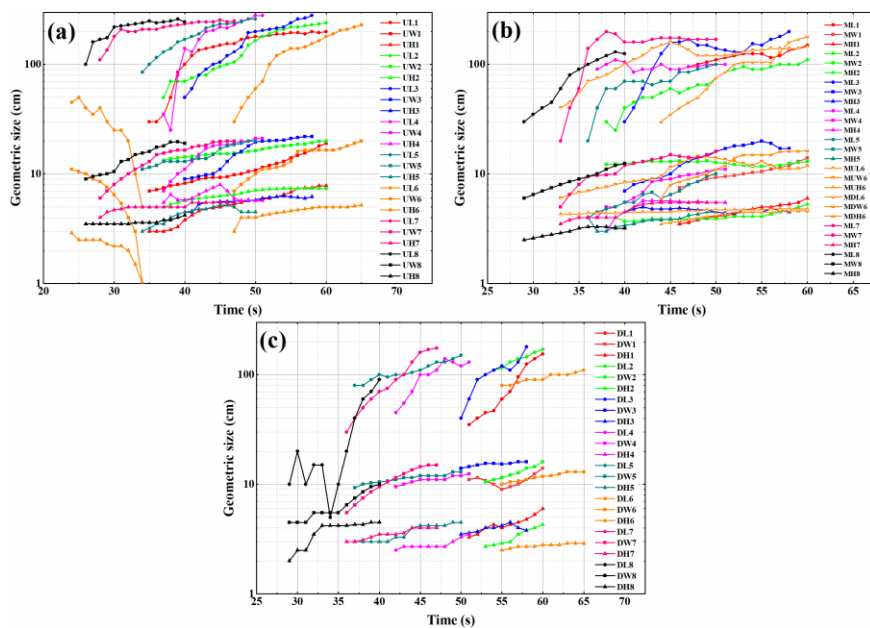
280 The positions of the upstream edges of type II and III boulder bar moved toward
 281 the dam toe during dam failure, but the downstream edges' positions could move toward
 282 or away from the dam. The distances of movement of the downstream edge positions
 283 were smaller than that of upstream edge positions. Compared with the boulder bars of
 284 type I, the movements of type II and III boulder bars were smaller. The distance between
 285 the boulder bars in the middle and downstream reaches is smaller than the distance
 286 between boulder bars near the upstream reaches and adjacent boulder bars.

287 3.3 Geometry size of the boulder bar during dam failure process

288 It is corresponding to Sect. 3.2, Fig. 6 shows that the lengths of the boulder bars
 289 of type I were longer than other types of boulder bars' lengths due to the sufficient
 290 incoming materials from the upstream dam. For all the boulder bars, their lengths along

291 the channel were largest, followed by widths, and lastly the heights. Boulder bars'
 292 lengths had a growing trend, and their growth rates were larger than widths and heights.

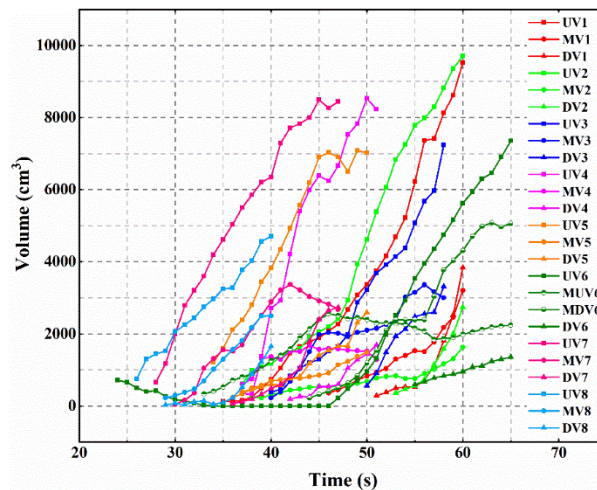
293 We recorded in detail the lengths, widths and heights of the boulder bars during
 294 the dam failure process at each moment (Fig. 6). The figure shows that boulder bars'
 295 heights changed less drastically than widths, which because boulder bars' heights were
 296 significantly affected by outburst flow depth. In most cases, flow depth was less than
 297 the heights of boulder bars. The sediments mainly accumulated at the boulder bars'
 298 edges and middle and could not "climb up" boulder bars' tops. Besides, the reduction
 299 of flow depth was not large enough, so the boulder bars' heights did not change seriously.
 300 The boulder bars' widths were significantly affected by the discharge of the outburst
 301 flow. When the discharge was enough, the sediments around the boulder bars were
 302 taken away by the flow, and the widths decreased. The variations of widths and heights
 303 both increase slowly with time and then tended to be stable values.



304
 305 **Figure 6.** The lengths, widths, and heights of the boulder bars: (a) sizes of the boulder bars near
 306 the upstream reaches; (b) sizes of the boulder bars near the middle reaches; (c) sizes of the boulder

307 bars near the downstream reaches. Notation: L, W, and H represent the length, width, and height of
 308 the boulder bar, respectively. *i* represents the *T_i* experiment. For example, MUL6 indicates the
 309 length of the boulder bar near the middle-upstream reaches for the T1 test.

310 When the amounts of sediments deposited on boulder bars were larger than the
 311 quantities of eroded sediments, boulder bars' volumes became larger. Otherwise,
 312 boulder bars' volumes would decrease or remain at a stable level. Figure. 7 reveals
 313 boulder bars' volume characteristic during the dam failure. Most of the 25 boulder bars
 314 gradually increased in volume, indicating that the amounts of outburst flow erosions in
 315 the boulder bars' vicinities were less than the amounts of siltation during the entire
 316 outburst process. Referred to Figs. 6 and 7, the boulder bars' volume characteristics
 317 were consistent with the boulder bars' length characteristics. And because the widths
 318 and heights developed slightly, boulder bars' volumes were mainly controlled by
 319 boulder bars' lengths.



320
 321 **Figure. 7.** Volumes of boulder bars. Notation: *UV_i*, *MV_i*, *DV_i*, *MUV_i*, *MDV_i* represent the volume
 322 of the boulder bar near the upstream reaches, the boulder bar near the middle reaches, the boulder
 323 bar near the downstream reaches, the boulder bar near the middle-upstream reaches, and the boulder

324 bar near the middle-downstream reaches, respectively. For example, UV1 means the volume of the
325 boulder bar near the upstream reaches of the T1 test.

326 **4. Geometry size of the boulder bars after dam failure**

327 In the Sec.3, we introduced formation characteristics and the geometry
328 characteristics of the boulder bars during the dam failure processes. In this section, we
329 will introduce the geometry characteristics of the boulder bar after the dam failure. After
330 the dam failure, there were 25 boulder bars formed along the channel for all the tests.
331 And it reflected the number of boulder bars was 0.4 to 1.0 times the ratio of river bed
332 length to dam bottom length. The parameter R is defined as the ratio of boulder bar
333 length L to width W in Eq. (1). And the dimensionless length L^* is calculated with Eq.
334 (2), where L_d is dam bottom length.

335 Figure 8(a) shows the relationship between R and the L^* of the 25 boulder bars
336 after the dams' failure in the experiments. The figure indicates that the values of R of
337 the boulder bars all fell within the range of 8 to 14. And, the R increases with the
338 increasing of L^* . However, the growth rate of R decreases as L^* goes by. The figures
339 show that there is a hyperbola relationship between R and L^* . The hyperbolic function
340 means that R would not sharply increase even become stable with the increasing of L^* .

$$R = \frac{L}{W} \quad (1)$$

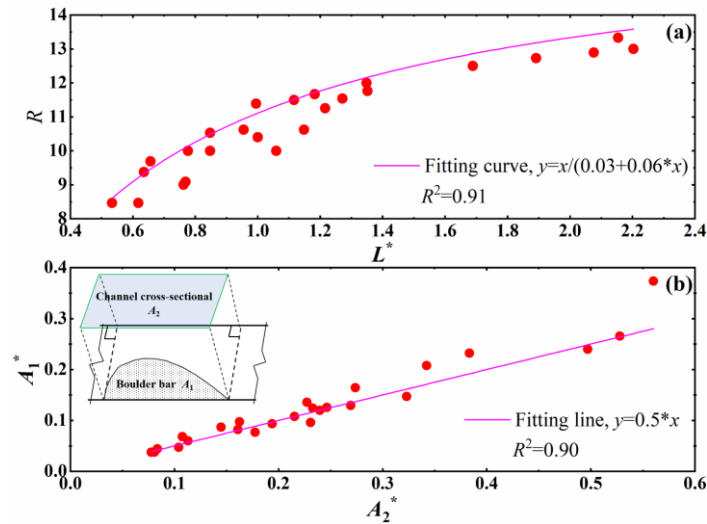
$$L^* = \frac{L}{L_d} \quad (2)$$

341 Two dimensionless parameters A_1^* and A_2^* are defined to reflect boulder bar's area

342 and channel cross-sectional area where the boulder bar located. They could be obtained
 343 by Eqs. (2) and (3) respectively. The relationship between A_1^* and A_2^* is shown in Fig.
 344 8(b). It can be seen that A_1^* increases as A_2^* increases. And there is a linear relationship
 345 between A_1^* and A_2^* . The figure suggests that the ratio of boulder bar's area to river
 346 channel cross-sectional area is approximately constant, which equals to 0.5.

$$A_1^* = \frac{A_1}{L_d^2} \quad (3)$$

$$A_2^* = \frac{A_2}{L_d^2} \quad (4)$$



347 **Figure.8.** Geometry characteristics of boulder bars after the dam failed in the experiments. (a)
 348 the relationship between length to width ratio (R) and dimensionless length (L^*); (b) the relationship
 349 between boulder bar's dimensionless area (A_1^*) and the cross-sectional dimensionless area of the
 350 river channel along the boulder bar (A_2^*).
 351

352 5. Discussion

353 In this paper, eight groups of landslide dam failure tests were conducted to

354 investigate the formation characteristics of boulder bars during the dam failure process,
355 and the geometry characteristics of boulder bars during and after the dam failure, which
356 are the main scientific objective of this paper. The experimental results are analyzed
357 and explained to meet the scientific objective. It should be noted that the materials of
358 riverbed and landslide dam were the same in the experiments. And the present
359 experiments are limited to homogeneous riverbeds and dams.

360 In order to verify the results of the experiments, data of 38 boulder bars in filed
361 formed by four landslide dam failures were used to compare the experimental data. It
362 noticed that the data of boulder bars during the landslide dam failure process are still
363 unavailable since the landslide dam mostly happened in inaccessible places and people
364 could not get there to record the field data in time. Therefore, the filed data in this paper
365 are all concerned about data after dam failure.

366 In this section, four field cases were used to verify the reliability of the boulder
367 bar distribution and geometry characteristics in this paper. In the Fig.9, boulder bars
368 were formed in the downstream river bed after Yigong landslide dam ($30^{\circ}10'38.07''$ N,
369 $94^{\circ}56'24.62''$ E), Tangjiashan landslide dam ($31^{\circ}50'26.79''$ N, $104^{\circ}25'51.17''$ E),
370 Sedongpu landslide dam ($29^{\circ}44'53.45''$ N, $94^{\circ}56'24.02''$ E), and Hongshihe landslide
371 dam ($32^{\circ}36'16.05''$ N, $105^{\circ}12'49.59''$ E) failed. The geometric data of boulder bars of
372 the four cases were obtained from Google Earth. The length of the river bed section we
373 selected was about 7 times of the dam bottom length. The detailed statistical data of
374 boulder bars shown as Table 3. It indicates that the number of boulder bars on the 17
375 km downstream river bed of the Yigong landslide dam was 2.67 times the ratio of the

376 river bed length to the dam bottom length; the number of boulder bars on the 5.6 km
 377 downstream river bed of the Tangjiashan landslide dam was 1.29 times the ratio of the
 378 river bed length to the dam bottom length; the number of boulder bars on the 6.4 km
 379 downstream river bed of the Sedongpu landslide dam is 0.57 times the ratio of the river
 380 bed length to the dam bottom length; and, the number of boulder bars on the 1.8 km
 381 downstream river bed of the Hongshihe landslide dam was 1.29 times the ratio of the
 382 river bed length to the dam bottom length. Generally, the number of boulder bars on the
 383 river bed for the four field cases are 0.57 to 2.67 times the ratio of the river bed length
 384 to the dam bottom length. These values are almost the same to the experimental values.

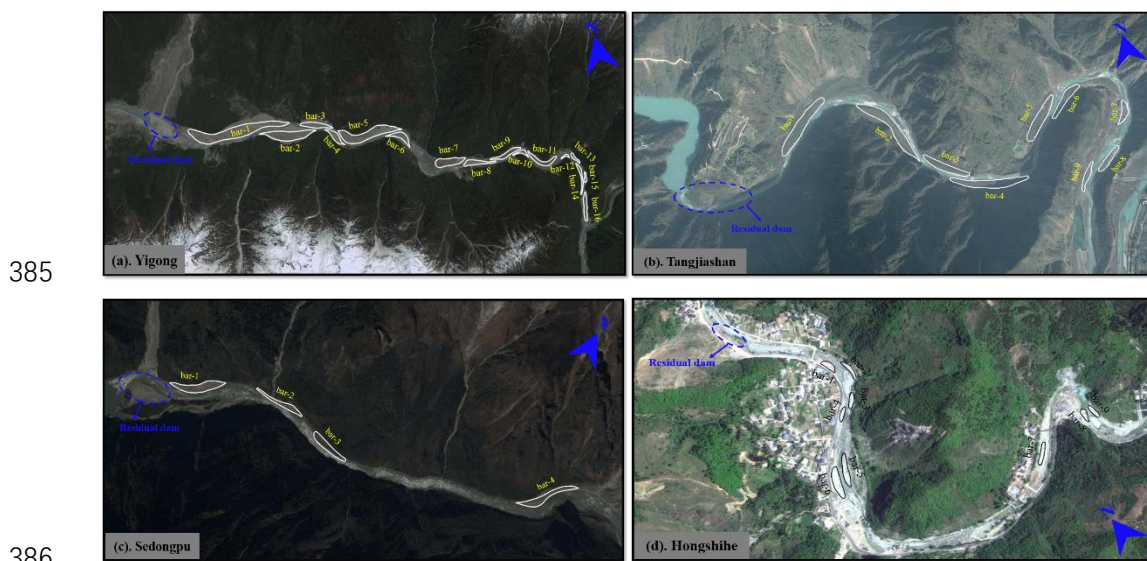


Figure.9. Google field images of four cases, © Google

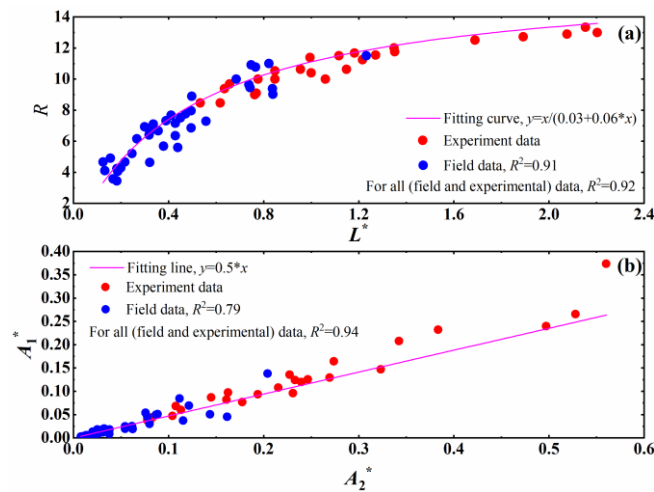
388 **Table 3** Field case data obtained through Google Earth. L_b is river bed length (m); L_d is dam bottom
 389 length (m); N is the number of boulder bars (-); R is the ratio of boulder bar's length to width (-).

Case		Data				
Landslide dam	Boulder bar	L_b	L_d	N	$N/(L_b L_d^{-1})$	R
Yigong	bar-1	17	2.800	16	2.67	11.50
	bar-2					9.45
	bar-3					6.35
	bar-4					4.63

	bar-5					9.38
	bar-6					5.69
	bar-7					5.59
	bar-8					7.76
	bar-9					7.67
	bar-10					4.66
	bar-11					7.15
	bar-12					4.67
	bar-13					4.91
	bar-14					6.59
	bar-15					4.11
	bar-16					6.67
Tangjiashan	bar-1					10.00
	bar-2					11.00
	bar-3					8.89
	bar-4					10.91
	bar-5	5.6	0.803	9	1.29	6.86
	bar-6					7.96
	bar-7					5.21
	bar-8					6.40
	bar-9					7.11
Sedongpu	bar-1					9.64
	bar-2	6.4	0.914	4	0.57	10.77
	bar-3					7.29
	bar-4					9.03
Hongshihe	bar-1					4.23
	bar-2					6.92
	bar-3					4.29
	bar-4					4.06
	bar-5	2.1	0.300	9	1.29	7.31
	bar-6					7.50
	bar-7					6.15
	bar-8					3.44
	bar-9					3.57

390 In addition, we also analyzed the data about R , L^* , A_1^* and A_2^* of the field boulder
391 bars. The Fig. 10(a) shows that the values of R of filed boulder bar all fall within the
392 range of 2 to 12, which are approximate to the range of values of the experimental
393 boulder bars. Furthermore, the hyperbola relationship in Fig. 8(a) is also suitable for
394 the field data in Fig. 10(a). And, both the experimental and filed data points are all

395 closed to the fitting curve, whose coefficient of determination (R^2) is 0.92. For the
 396 boulder bars in the field, A_1^* and A_2^* show a linear relationship, and the fitting equation
 397 of the experimental data (Fig.8 (b)) is very suitable for the field data in Fig.10 (b). It
 398 means that the fitting line could predict the relationship between A_1^* and A_2^* for both
 399 experimental and field boulder bar well (the coefficient of determination is 0.94).



400
 401 **Figure.10.** Geometry characteristics of boulder bars after the dam failed in the field. The
 402 experimental data are also plot in the figure to compare to the field data. (a) The relationship between
 403 boulder bar length to width ratio (R) and dimensionless length (L^*); (b) The relationship between
 404 boulder bar's dimensionless area (A_1^*) and the cross-sectional dimensionless area of the river
 405 channel along the boulder bar (A_2^*).

406 Based on the above points, it can be seen that the experimental results in this paper
 407 are consistent with the actual boulder bars in the field. Therefore, the experimental
 408 results can provide references for the field study of the boulder bar formed by the
 409 outburst flood triggered by landslide dam failure. The results in this paper can help
 410 researchers deepen their understanding of river channel's geomorphological variation
 411 characteristics affected by the outburst flood, and provide a data reference for the

412 analysis of the erosion and accumulation characteristics of the downstream river
413 channel. Especially, with these two relationships, i.e., $R-L^*$ and $A_1^*-A_2^*$, the boulder bars
414 geometry size could be predicated after a landslide dam formation in the future. Then
415 the new landform after the dam failure could be evaluated. These presentations could
416 contribute to the stream restoration planning, river navigation, and even utilization
417 planning of the boulder bars.

418 **Conclusion**

419 In this paper, a downstream moveable bed for 4 to 7 times the length of landslide
420 dam length along the channel was set, and through eight flume experiments, 25 boulder
421 bars were formed downstream channel caused by overtopping flow. The boulder bar's
422 formation process and geometry characteristics are studied. The main conclusions are
423 as follows.

424 (1) Boulder bars first appear near dam toes (upstream reaches located on the dam's
425 initial breach sides). Inertia force made sediment accumulate on the opposite banks of
426 the channel bed, resulting in boulder bars' formations downstream. During the landslide
427 dam failure process, the boulder bars' upstream edges are mainly in siltation states. The
428 boulder bars' lengths increase with failure time, mainly caused by boulder bars'
429 upstream edges move upstream. The downstream edges develop slowly and basically
430 near the initial positions. And the developments of boulder bars' downstream edges are
431 much smaller than the developments of boulder bars' upstream edges.

432 (2) During the dam failure process, the lengths varied faster than the widths and

433 heights of boulder bars. And the boulder bars' lengths along the river are the largest,
434 followed by widths, and lastly the heights when the dam completed failed. The volumes
435 of the boulder bars increase with dam failure, and boulder bars' volume characteristics
436 are consistent with boulder bars' lengths characteristics.

437 (3) In the experiments, the ratio (R) of boulder bar length to width falls at the range
438 of 8 to 14. There is a nonlinearly relationship between length to width ratio (R) and the
439 dimensionless length of boulder bar (L^*), which could be described as a hyperbolic
440 equation. The dimensionless area (A_1^*) of boulder bar has a linear relationship with the
441 dimensionless area (A_2^*) of the channel cross section, whose slope is about 0.5.

442 (4) In this paper, 38 boulder bars in the field triggered by four landslide dams'
443 failures were investigated. By comparing the data of boulder bars in field with the
444 boulder bars in the experiments, the distribution and geometric size characteristics of
445 the boulder bars in the field are more consistent with the boulder bars in the experiments,
446 indicating that the experimental results are more reliable.

447 **Author contribution**

448 Xiangang Jiang was responsible for the experiments, article thinking, and writing.
449 Haiguang Cheng was responsible for calculating the article parameters. Lei Gao was
450 responsible for the article's pictures, and Weiming Liu was responsible for checking the
451 full article.

452 **Competing interests**

453 The authors declare that they have no known competing financial interests or

454 personal relationships that could have appeared to influence the work reported in this
455 paper.

456 **Acknowledgments**

457 This research has been supported by The National Natural Science Foundation of
458 China (No. 41807289) and Key Laboratory of Ministry of Education for Geomechanics
459 and Embankment Engineering, Hohai University (No. 202020) and Open fund of Key
460 Laboratory of mountain hazards and surface processes, Chinese Academy of Sciences
461 (No. KLMHESP-20-05).

462 **Code and data availability statement**

463 The codes and data that support the findings of this study are available from the
464 corresponding author upon reasonable request.

465 **Reference**

- 466 Ashworth, P. J.: Mid-channel bar growth and its relationship to local flow strength and
467 direction, *Earth Surf. Process. Landforms*, 21, 103-123,
468 [https://doi.org/10.1002/\(SICI\)1096-9837\(199602\)21:2<103::AID-
469 ESP569>3.0.CO;2-O](https://doi.org/10.1002/(SICI)1096-9837(199602)21:2<103::AID-ESP569>3.0.CO;2-O), 1996.
- 470 Ashworth, P. J., Best, J. L., Roden, J. E., Bristow, C. S., and Klaassen, G. J.:
471 Morphological evolution and dynamics of a large, sand braid-bar, Jamuna River,
472 Bangladesh, *Sedimentology*, 47 (3), 533-555, [https://doi.org/10.1046/j.1365-
473 3091.2000.00305.x](https://doi.org/10.1046/j.1365-3091.2000.00305.x), 2000.

474 Benito, G. and O'Connor, J. E.: Number and size of last glacial Missoula floods in the
475 Columbia River valley between the Pesco Basin, Washington, and Portland,
476 Oregon. Geological Society of America Bulletin, 115, 624 –638,
477 [https://doi.org/10.1130/0016-7606\(2003\)115<0624:NASOLM>2.0.CO;2](https://doi.org/10.1130/0016-7606(2003)115<0624:NASOLM>2.0.CO;2), 2003.

478 Carling, P. A.: Freshwater megaflood sedimentation: what can we learn about generic
479 processes? Earth-Science Reviews, 125, 87113,
480 <https://doi.org/10.1016/j.earscirev.2013.06.002>, 2013.

481 Casagli, N., Ermini, L. and Rosati, G.: Determining grain size distribution of the
482 material composing landslide dams in the Northern Apennines: Sampling and
483 processing methods, Engineering Geology, 69, 83-97,
484 [https://doi.org/10.1016/S0013-7952\(02\)00249-1](https://doi.org/10.1016/S0013-7952(02)00249-1), 2003.

485 Chen, S. C., Lin, T. W. and Chen, C. Y.: Modeling of natural dam failure modes and
486 downstream riverbed morphological changes with different dam materials in a
487 flume test, Engineering Geology, 188, 148-158,
488 <https://doi.org/10.1016/j.enggeo.2015.01.016>, 2015.

489 Costa, J. E. and Schuster, R. L.: The formation and failure of natural dams, Geol Soc
490 Am Bull, 100(7), 1054-1068, [https://doi.org/10.1130/0016-7606\(1988\)100<1054:TFAFON>2.3.CO;2](https://doi.org/10.1130/0016-7606(1988)100<1054:TFAFON>2.3.CO;2), 1988.

492 Jiang, X. G., and Wei, Y. W.: Natural dam breaching due to overtopping: effects of
493 initial soil moisture, Bull Eng Geol Environ 78, 4821–4831,
494 <https://doi.org/10.1007/s10064-018-01441-7>, 2018.

495 Jiang, X. G.: Laboratory Experiments on Breaching Characteristics of Natural Dams on

496 Sloping Beds, *Advances in Civil Engineering*, 5064093, 14,
497 <https://doi.org/10.1155/2019/5064093>, 2019.

498 Jiang, X. G. and Wei, Y. W.: Erosion characteristics of outburst floods on channel beds
499 under the conditions of different natural dam downstream slope angles, *Landslides*,
500 1-12, <https://doi.org/10.1007/s10346-020-01381-y>, 2020.

501 Lamb, M. and Fonstad, M.: Rapid formation of a modern bedrock canyon by a single
502 flood event. *Nature Geosci*, 3, 477 –481, <https://doi.org/10.1038/ngeo894>, 2010.

503 Maizels, J. K.: Jökulhlaup deposits in proglacial areas. *Quaternary Science Reviews*,
504 16, 793 –819, [https://doi.org/10.1016/S0277-3791\(97\)00023-1](https://doi.org/10.1016/S0277-3791(97)00023-1), 1997.

505 Marren, P. M. and Schuh, M.: Criteria for identifying jökulhlaup deposits in the
506 sedimentary record. In: Burr, D.M., Carling, P.A., Baker, V.R. (Eds.),
507 *Megaflooding on Earth and Mars*, Cambridge University Press, 225-242,
508 <https://doi.org/10.1017/CBO9780511635632>, 2009.

509 Mohrig, D., and Smith, J. D.: Predicting the migration rates of subaqueous dunes, *Water*
510 *Resources Research*, 32 (10), 3207-3217, <https://doi.org/10.1029/96WR01129>,
511 1996.

512 Morris, M. and Hassan, M., Kortenhaus, A., Geisenhainer, G., Visser, P.J., and Zhu,
513 Y.: Modelling breach initiation and growth, Munich: HR Wallingford, 1(5):175-
514 185, 2009.

515 Peng, M. and Zhang, L. M.: Breaching parameters of landslide dams, *Landslides*, 9, 1,
516 13-31, <https://doi.org/10.1029/2018WR024107>, 2012.

517 Russell, A. J. and Knudsen, O.: Controls on the sedimentology of the November 1996
518 jökulhlaup deposits, Skeiðarársandur, Iceland. In: Smith, N.D., Rogers, J. (Eds.),
519 Fluvial sedimentology VI. Special Publication of the International Association of
520 Sedimentologists, 28, 315 –329, <https://doi.org/10.1002/9781444304213.ch23>,
521 1999.

522 Shaw, J. B., and McElroy, B.: Backwater number scaling of alluvial bed forms, J.
523 Geophys. Res. Earth Surf, 121, 1436– 1455, doi:[10.1002/2016JF003861](https://doi.org/10.1002/2016JF003861), 2016.

524 Takahashi, T.: Debris flow Mechanics, Prediction and Countermeasures, Taylor and
525 Francis Group, 35-38, <https://doi.org/10.1201/9780203946282>, 2007.

526 Turzewski, M. D., Huntington, K. W. and LeVeque, R. J.: The Geomorphic Impact of
527 Outburst Floods: Integrating Observations and Numerical Simulations of the
528 2000 Yigong Flood, Eastern Himalaya. Journal of Geophysical Research: Earth
529 Surface, 124, 1056-1079, <https://doi.org/10.1029/2018JF004778>, 2019.

530 Wu C. H., Hu, K. H., Liu, W. M., Wang, H., Hu, X. D., and Zhang, X. P.: Morpho-
531 sedimentary and stratigraphic characteristics of the 2000 Yigong River landslide
532 dam outburst flood deposits, eastern Tibetan Plateau, Geomorphology, 107293,
533 <https://doi.org/10.1016/j.geomorph.2020.107293>, 2020.

534 Zhou, G. G. D., Zhou, M. J., Shrestha, M. S., Song, D. R., Choi, C. E., Cui, K. F. E.,
535 Peng, M., Shi, Z. M., Zhu, X. H., and Chen, H. Y.: Experimental investigation on
536 the longitudinal evolution of landslide dam breaching and outburst floods,
537 Geomorphology, 334, 29-43, <https://doi.org/10.1016/j.geomorph.2019.02.035>,
538 2019.